Counter-intuitive Adsorption of $[PW_{11}O_{39}]^{7-}$ on Au(100)

Zhongling Lang,[1] Xavier Aparicio-Anglès,[2] Ira Weinstock,[3] Anna Clotet,[1] and Josep M. Poblet[1]**

1. *Departament de Química Física i Inorgànica, Universitat Rovira i Virgili,c/Marcel·lí Domingo 1, 43007 Tarragona, Spain.*

2. *Department of Chemistry, University College London, WCH1 0AJ, London, United Kingdom.*

3. *Department of Chemistry, and the Ilse Katz Institute for Nanoscale Science & Technology, Ben-Gurion University of the Negev, POB 653, Beer Sheva, 84105. Israel.*

KEYWORDS: Polyoxometalates; DFT; gold surface.

ABSTRACT: To understand the interaction between charged species and surfaces is one of the most challenging topics in chemistry, given its wide involvement in several fields such as electro-catalysis, stabilization of metal nanoparticles (NPs), or preparation of devices, among others. In general, these systems are particularly complex to model due to the elevated number of factors that have to be taken into account. Here, we report a robust strategy based on DFT to study these interactions, which has been applied to the highly charged lacunary $[PW_{11}O_{39}]^{7-}$ (PW_{11}) adsorbed on gold and silver surfaces. In this context, we find that, unlike the modelling of poloxoanions in solution, the incorporation of counterions in the computational models is crucial

to accurately reproducing the properties of the system, even if an implicit solvent is used. Most interestingly, we find that the PW_{11} cluster does not preferentially adsorb onto the gold surface *via* its more nucleophilic mono-defect face, but rather, through less negatively charged terminal oxygen ligands, with an orientation similar to that found for the non-defective Keggin anion $[SiW_{12}O_{40}]^{4-}$, induced by the strong anion-cation interactions from the same and neighboring units. This counter-intuitive result is important in ongoing efforts to understanding and utilizing the properties of polyoxometalate monolayers on gold and other reactive metal surfaces.

INTRODUCTION

Polyoxometalates (POMs) are metal-oxide clusters, typically formed *via* the self-assembly of $\{MO_x\}$ blocks (M = Mo^{VI}, W^{VI}, V^{V}, Nb^{V}, Ta^{V}, *etc*.) and $\{XO_4\}$ (X = P^{V}, Si^{IV}, As^{III}, S^{VI}, *etc*.) polyhedra in aqueous solution.[1-3] The particular properties of POMs, such as redox potentials, acidity, or stability among others,[4-7] enabled their applications in catalysis and material science.[8] Nowadays, one of the main hot-topics regarding polyoxometalates is to combine them with other components possess interesting properties, in order to obtain functional composite materials. The simplest and more effective way is to adsorb them on planar surfaces or metal nanoparticles (NPs).[8] The deposition of polyoxometalates on electrodes has been extensively exploited by Nadjo and Keita *et al*. in order to modify the properties of the electrodes for catalytic activity study.[9] Anson *et al*., Keita *et al*., Gewirth *et al,* and others have investigated the POMs grafting on planar-metal or graphite, demonstrating the formation of POM monolayers with well-defined packing structures.[10-12]

The polyoxometalates can also adsorb on NPs by the work of Frank,[13] and paved the way to utilize these POM-NPs nanostructures in catalyst.[14] Moreover, a recent work has provided a direct

correlation between the electronic effects of the POMs (including PW_{11}) bound to the surfaces of the gold nanoparticles, and rates of CO oxidation by O_2.[15] The role of POMs in composite materials is not only limited to improving catalytic activities, but also encompasses other functions. For example on NPs, POMs act as stabilizing agents,[14] leading to the formation of organized self-assembled monolayers (SAM).[8, 16-17] Weinstock *et al*. pointed out that the stability of POM SAMs on metal NPs, observed by Cryo-TEM images,[18-21] was largely dependent on the nature of the counter-cations, understood to be structurally integrated into the POM-NP composite. Whether the adsorption takes place on a flat surface or on a metal nanoparticle, the interaction between moieties is central to understand the final properties of the material.

A good example of that is the stabilization of gold nanoparticles by means of the defective lacunary anion $[XW_{11}O_{39}]^{n-}$ ($X=P^{V}$, Si^{IV}, Al^{III}).[18-21] As depicted in Figure 1, the $[XW_{11}O_{39}]^{n-}$ mono-defective (lacunary) POM is formed by removing one single WO^{4+} unit from the complete Keggin structure, thereby resulting in a remarkable increase of the charge. The extra charge is not uniformly distributed and it is slightly concentrated at the defective region or lacuna. Hence, the lacuna is more reactive,[1] and allows the lacunary POM either to act as intermediate species in the transformation of molecular metal oxides,[22] or its functionalization with more active moieties.[23]

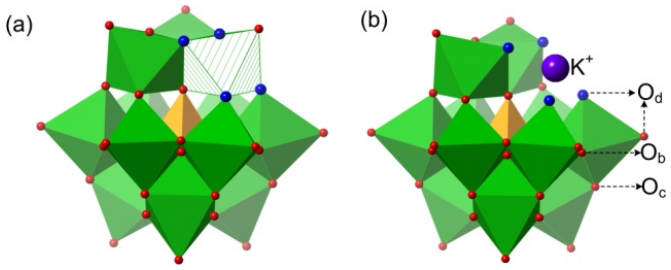

Figure 1. Polyhedral-ball representations of (a) a generic Keggin anion $[\alpha\text{-}PW_{12}O_{40}]^{3-}$, and (b) its mono-defect (or lacunary) derivatives $[\alpha\text{-}PW_{11}O_{39}]^{7-}$ (PW_{11}) with one K^+ filled in the lacuna. Color code: tungsten (green), oxygen (red, and the four oxygen at the lacuna site were labeled as blue), phosphorus (orange), potassium (violet).

Using cryo-TEM images, it has been revealed that the $\alpha\text{-}[AlW_{11}O_{39}]^{9-}$ (AlW_{11}) can stabilise Ag(0) and Au(0) NPs by deposition on their surface,[18-19] and it has also provide valuable information about the thickness of the POM interface and the separation between AlW_{11}.[21] Given the more nucleophilic character of the lacuna, it would be expected that the AlW_{11} was adsorbed *via* this side. Unfortunately, the cryo-TEM images could not confirm or disprove this hypothesis, despite their strong potential in elucidating structural information. Rather, solution-state binding studies suggested that total POM charge, rather than specific binding of the nucleophilic lacunae site, was most important in determining the stabilities of POM monolayers on gold nanoparticles.[8, 19-21] More detailed understanding of this counter-intuitive result would provide valuable information about the nature of interactions between POMs and surfaces.

The computational modelling of these systems represents a milestone in understanding the interaction and the resulting properties of these materials. Only a few studies have been reported in this area,[24-29] our group has focused on the modelling of POMs deposited onto the metallic surfaces and tried to identify the main factors that are necessary to take into account in the modelling.[25, 30] We have shown that the reduction of $[SiW_{12}O_{40}]^{4-}$ on the Ag surface can be reproduced only if the environmental effects from both cations and solvent are taken into account by combining density functional theory (DFT) calculations with molecular dynamic (MD)

simulations.[25b] However, this approach is quite computationally demanding and not very efficient for calculating energy differences.

Hence, in the current work we present an improved and more robust computational strategy for the modelling of ionic species on surfaces. Using the PW_{11} as test system, we are intend to discuss about the possible adsorption orientations, electronic properties, and the nature of the interaction between the PW_{11} and the Au(100) surface in both vacuum and solution. We benchmark our strategy with the full Keggin anion $[SiW_{12}O_{40}]^{4-}$ and silver surface, which then allows us to determine the main factors that have to be considered in modelling ions on surfaces.

COMPUTATIONAL DETAILS AND MODELS

Computational details

All first principle calculations were performed using the Vienna *ab*-initio simulation package (VASP5.3), which is based on periodic DFT, using plane waves as a basis set.[31] Based on our previous work, we set the kinetic energy cut-off at 500 eV, and used the Perdew–Wang 91 functional (PW91) to describe the exchange correlation potential.[32] Per species, the valence electrons considered were the following: $5d^{10}6s^{1}$ for Au, $4d^{10}$ $5s^{1}$ for Ag, $3p^{6}4s^{1}$ for K, $2s^{2}2p^{4}$ for O, $3s^{2}3p^{3}$ for P, and $5d^{4}6s^{2}$ for W. The interaction between these valence electrons and the corresponding pseudopotential was described using the projector augmented wave (PAW) scheme with scalar relativistic effects.[33] All the models are relaxed by keeping the bottom three Au layers fixed at their bulk truncated position. All optimizations were performed until self-consistence, with thresholds of $1 \cdot 10^{-5}$ eV and $3 \cdot 10^{-2}$ $eV \cdot A^{-1}$ for the electronic and the ionic convergence respectively. The reciprocal space was described using two different Monkhorst Pack Schemes[34]: 3 × 3 × 1 for structure optimizations, and 5×5×1 for calculating the density of states (DOS). Bader's AIM (Atoms in Molecules) atomic charges[35] were determined using the

Henkelmann algorithm.[36] Solvent effects were included by means of the implicit solvation model (named VASPsol) implemented by Hennig and co-workers.[37] In addition,frequency calculations were performed to ensure the stability of each model. Finally, a data set collection of computational results is available in the ioChem-BD repository[38] and can be accessed via http://dx.doi.org/10.19061/iochem-bd-2-10 (http://www.iochembd.org/).

Model

Regarding the average distance between the centers of the neighboring POM anions is about 1.57±0.04 nm in experiment,[19] the gold surface was modeled in a high coverage situation by using the 5×5 Au (100) slab model, consisting of four gold layers with 25 gold atoms per layer. The calculated lattice parameter for the gold bulk was 4.17 Å, which is in a reasonable agreement with the experimental bulk parameter of 4.07 Å.[39,40] Accordingly, the dimensions of the unit cell were 14.76 Å for *a* and *b* directions, corresponding to the P···P distance of the neighboring POM anions. The *c* direction was set at 35.17 Å, considering a vacuum space of more than 15 Å, which was proven to be sufficient to avoid the interactions between the replicated cells. All isolated molecules were calculated in a cubic box of side 25 Å.

We have considered three different adsorption orientations for PW_{11}: S_4, C_3, and lacuna with maximum number of Au-O_d connections and the optimized orientations are depicted in **Figure 2**. Notice that although we use S_4 and C_3 rotational axes for labeling the two adsorption modes, they are formally present in the $[\alpha\text{-}PW_{12}O_{40}]^{4-}$ but not in the PW_{11}. In addition, we did not take into account different adsorption sites nor rotations of the POM on the surface because we proved that the main properties of the system are not strongly influenced by these two factors.[25]

The charge of the POM was compensated using potassium atoms displayed around the POM, and the solvent was modeled using an implicit model with dielectric constant of water as $\varepsilon = 80$.[37]

By locating the equal number of K atoms around the POM, the neutral POM is very likely to accept the valence electron of K, thus resulting the K^+ and POM^{7-}. In our study, the vacuum and the implicit solvent situations are symbolized as two extreme situations. The vacuum represents an ideal situation in which the surface, the POM, and the counterions are completely dehydrated, whereas the solvent model represents a situation in which all the species are in contact with the solvent. We designate these extreme situations as "*dry*" and "*wet*" surfaces.

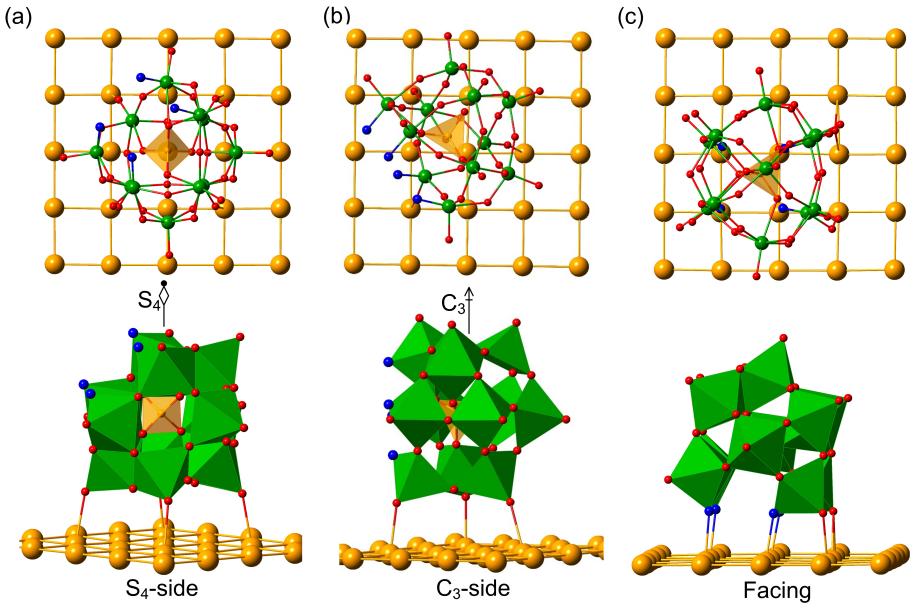

Figure 2. Ball-stick (top) and polyhedral (bottom) representations of the optimized geometries for PW_{11} deposited on the Au(100) surface via a) the S_4 improper rotation axis, b) C_3 proper rotation axis, and c) with the lacuna facing the surface.

RESULTS AND DISCUSSION

Cation distribution around the $[PW_{11}O_{39}]^{7-}$ anion

The first step is to determine the potential cation distribution around the PW_{11} anion. To that end, we performed molecular dynamic simulations with the POM using the DL_POLY code in a

saturated solution, which are discussed in the ESI.[41-44] From the MD simulations (Figure **S1**), we observed that in solution the lacuna was always filled with one counterion and a second counterion could also be located near to PW_{11} for a short period of time. Unfortunately, the rest of counterions were found between 12.0 and 45.0 Å away from the PW_{11}, which was not close enough to fit the whole system in the surface unit cell. From these calculations, we can deduce that cations are, on average, at large distances from the POM.

In order to fit the POM and the counterions on the surface unit cell, we screened different potassium distributions around the adsorbate at very short distances using DFT, so ensure that they will be close enough. We optimized seven cation distributions (labeled from **A** to **G**), which differ in the position of the counterions. These positions are: the quartet O_4, the O_b triads, the O_c triads, and the lacuna (detailed in Fig. **S2**). Optimization was performed in the vacuum and using implicit solvent, and the system's relative energies are collected in Table 1. In addition, a full description of the different sites, nomenclature, and cation distributions can be found in Figure S2 in the ESI.

In the vacuum, the total energy of the K_7PW_{11} system is highly influenced by the cation distribution, as evidenced by the large range of energies, which is around 69 kcal·mol^{-1}. The most stable structure, **A**, has one cation at the lacuna, four near the O_4-site and two near O_4–1 site. In fact, molecular dynamic simulations already suggested that these two sites would be occupied by cations. The rest of structures were found between 23 and 69 kcal·mol^{-1} higher in energy.

However, in solution the range of relative energies is only 12.0 kcal·mol^{-1}, implying that the energy of the system is less sensitive to the cation distribution. These findings are reasonable since in solution, POM and counterions are surrounded by their respective solvation spheres, shielding their ionic interaction.[45,46,47] Regardless, structure **A** is still the most stable distribution.

We also observe that for those structures lower in energy (**A**, **D**, and **F**), one cation is placed at the lacuna, in agreement with the observations obtained from the molecular dynamic simulations. However, in solution the difference in energy between the structures with a cation and those without a cation on the lacuna is significantly smaller.

Table 1. Relative energies (in kcal·mol^{-1}) for the different cation distributions around the POM in vacuum and with implicit solvent.

K distribution	ΔE (vacuum)[a]	ΔE(solution)[b]
A	0.0	0.0
B	23.5	6.2
C	55.8	12.0
D	31.6	5.1
E	68.9	12.0
F	27.0	5.3
G	27.7	9.7

a) System consists of POM+7K; b) In solution the solvent is simulated by a continuum model.

Adsorption of $K_7PW_{11}O_{39}$ on the Au(100) surface

Assuming the three adsorption modes represented in Fig. 2, we have explored the following systems, labeled from 1) to 6) as: 1) S_4–K, 2) S_4, 3) C_3–K, 4) C_3, 5) Facing-K, and 6) Facing respectively, where "(*mode*)–K" indicates that one K^+ is directly linked to the four terminal oxygens of the lacuna. Additionally, the other K^+ are arbitrarily distributed around the POM. The detailed information of the models is shown in Figure **S3**.

In vacuum, Au–O_d distances were found in a range between 2.52 and 2.69 Å, and slightly larger values, between 2.59 and 2.72 Å, for the solvated surface, as shown in Table 2. These distance ranges agreed with the experiments regarding the adsorption of $[AlW_{11}O_{39}]^{9-}$ on gold NPs, in which that range was set to be between 2.5 and 3.0 Å.[21] The only exception was for the Facing-K (system 5 in Table 2), which showed an average distance of 3.67 Å, more than 1 Å longer than

the other structures. In this case, however, this enlargement is a consequence of the K^+ placed at the lacuna.

The K–O distances enlarged when the solvent was included in the calculations, from 2.69-2.77Å to 2.92-2.97Å. This increase is a consequence of the stabilization that the solvent exerts onto the PW_{11} anion and the counterions. Finally, the W–O_d distances, referring to those O_d that are closest to the surface, showed almost no change with respect to the non-adsorbed PW_{11} (1.75Å), evidencing the poor affinity that POMs and gold surfaces have, in contrast to silver surfaces.[25]

Table 2. Selected distances (in Å) for different POM adsorption orientations (**1** to **6**) on "*dry*" (*Vac*.) and "*wet*" (Sol.) surface. [a]

Sites	Phase	Au–O_d	Au–O_d (av)	K–O (av)	W–O_d (av)
(1) S_4–K	Vac.	2.58-2.67	2.61	2.69	1.74
	Sol.	2.68-2.81	2.72	2.92	1.75
(2) S_4	Vac.	2.53-2.69	2.60	2.77	1.75
	Sol.	2.56-2.71	2.62	2.97	1.75
(3) C_3–K	Vac.	2.37-2.75	2.59	2.74	1.75
	Sol.	2.50-2.70	2.60	2.92	1.75
(4) C_3	Vac.	2.29-2.75	2.59	2.74	1.77
	Sol.	2.32-2.91	2.67	2.97	1.75
(5) Facing– K	Vac.	3.36-3.94	3.67	2.75	1.79
	Sol.	3.66-3.96	3.80	2.92	1.77
(6) Facing	Vac.	2.42-2.69	2.52	2.74	1.76
	Sol.	2.44-2.88	2.59	2.93	1.76

a) Au– O_d ($O_{d\,(av.)}$) is the distance (average) between those O_d and the contact Au atoms. The K–$O_{(av)}$ is the average distance between K^+ and the nearby oxygen (less than 3.5 Å). As well, W-$O_{d\,(av)}$ refers to those O_d in contact with the surface.

As we observed for the non-adsorbed PW_{11}, the more stable systems in vacuum are those that have the lacuna filled with one K^+, all found in a range of 3.2 kcal·mol^{-1}, regardless of their adsorption orientation (Table 3 and Figure 3). On the other hand, those structures that do not have a K^+ at the lacuna are found between 6.0 and 30.2 kcal·mol^{-1} with respect to the most stable system. Interestingly the most unstable system is the *Facing* with no K^+. This is also counter-intuitive, as anionic protecting ligands might be assumed to directly interact with the gold surface via their most negatively charged regions, as shown by the molecular electrostatic potential representation of the free anion in Figure S4. According to these results, however, the key factor in stabilizing the system in vacuum is the presence of the counterion in the lacuna and not the adsorption orientation. Notably, this is supported by experimental data by Weinstock, who showed that POM charge, rather than structure (*i.e.*, the presence or absence of a lacunary site) controls the thermodynamics of POM-monolayer assembly on Au NPs.[8, 19-21] In the same direction, Finke has shown that the complete Nb substituted Wells-Dawson anion, $[P_2W_{15}Nb_3O_{62}]^{9-}$, is more effective for the formation and stabilization of Ir(0) NPs, than the lacunary anion $\{H[\alpha_2\text{-}P_2W_{17}O_{61}]\}^{9-}$ with the equal charge.[48] In other words, the presence of lacunary site in the POM framework appears to produce no special effect on the stabilization of Ir(0) NPs.

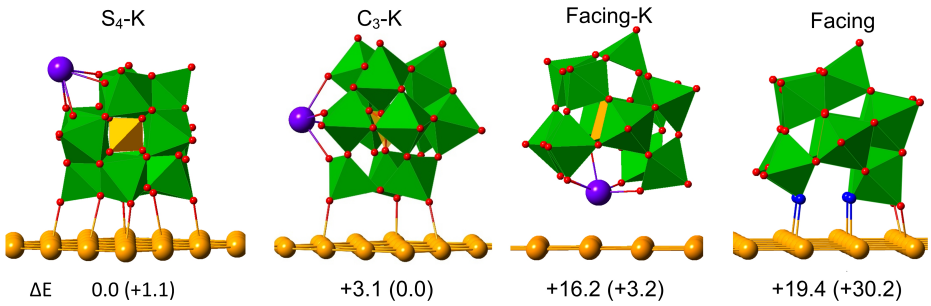

Figure 3. 3D representations and relative energies (in kcal·mol^{-1}) for some selected structures. Values in parenthesis are relative energies computed in vacuum, see text.

In solution, results are somewhat different because now the difference in energy between having the lacuna filled or not is very small, although the former is still more stable than the latter. When the implicit solvent is included, the S_4 orientation with the K^+ fully exposed to the solvent (Figure 3) becomes the most stabilized form. The C_3 form is slightly higher in energy because the cation is in less contact with the solvent, especially if we are dealing with a high coverage situation, and finally the facing-K form is quite high in energy (+16.2 kcal·mol^{-1}) because the cation in no way can interact with the solvent. This means that on gold surfaces the lacunary anions will try to have the cations in contact with the solvent and as a general behavior the linkage with the surface will be similar to that of the complete anions.

In order to further understand the reasons that explain the orientation of the POM on metal surface, we have analysed the variation in the charge density upon adsorption for S_4-K and Facing systems in solution, by subtracting the electronic charge of a $K_7PW_{11}O_{39}$/Au(100) system from its components $K_7PW_{11}O_{39}$ and Au(100). As expected, adsorption of the POM induces a positive image charge in the gold region in contact with the adsorbed anion, fact that is manifested by an electron density reduction in Figure 4. In the representation of charge density dfferences we have used very low isovalues in order to visualize better the small electron density

reorganization induced by the adsorption of POMs on gold surfaces. Similar effects are observed in the gold atoms near counterions, but that regions show charge accumulations because of the positive charge of the cations. However, no electron accumulations are observed in the bonding Au-O region discarding any covalent interaction between gold surface and POM for any of the orientations of the anion, the main interaction being of electrostatic nature. A lesser electron deficit in S_4-K, leading to a weaker electrostatic attractive than that in Facing.

However, it is important to remark that anion-cation interactions are very relevant in the adsorption process as it has already been revealed previously.[20] Furthermore to the stabilization generated when a K^+ occupies the defect site in S_4-K, additional interactions between K^+ ions neighboring units are vey important, in particular four K^+ strongly interact at the same time with two anions as shown in Figure S5. In this context, we have verified that the relative stability of S_4-K and Facing adsorptions decreases from 19.4 up to 5.3 kcal·mol^{-1} when the calculations are performed in solution with two POMs separated enough to avoid the interactions of POM···K···POM type. In the low coverage situation, the P···P distance between two neighboring POMs is about 23.6 Å, whereas for the high coverage represention that value is only 14.8 Å. Therefore, the strong cation-anion interactions, especially the donation from the defect site, bring more stability rather than the electrostatic interactions, leading to the S_4-K orientation more favourable than Facing.

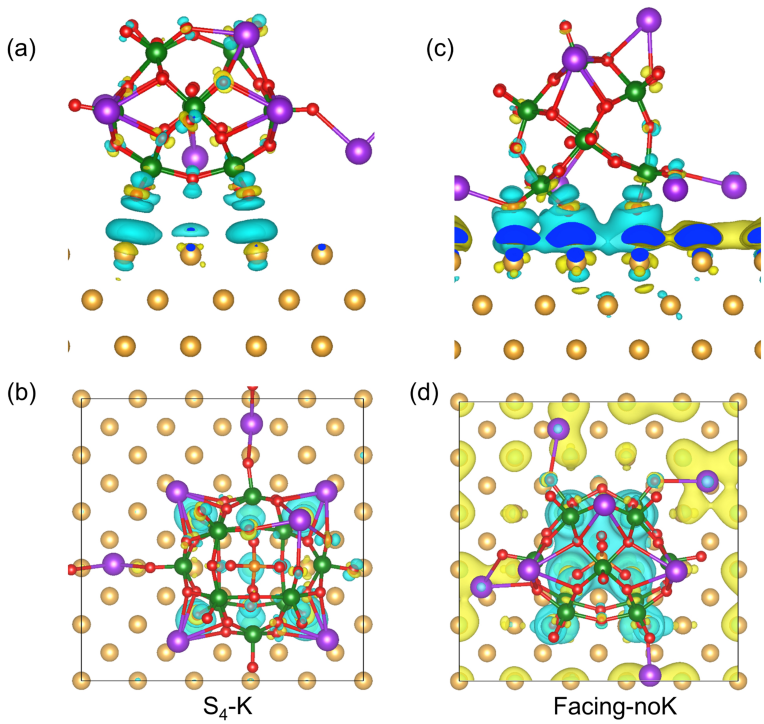

Figure 4. Three-dimensional charge density difference for S_4-K (a, b), and Facing (c, d) systems with views from side and top, respectively, $\varrho_{diff}(r) = \varrho_{K7POM/Au(100)}(r) - \varrho_{K7POM}(r) - \varrho_{Au(100)}(r)$. The yellow region represents charge accumulations (electron density increase), and the cyan regions indicates charge depletion (electron density decrease). The isovalue is set to 0.001 e/Bohr^3 in Vesta code.[49] And the maxmum to minimum charge difference in S_4-K is -0.013~0.005 e/Bohr^3 and -0.025~0.011 e/Bohr^3 for Facing.

Affinity of Au(100) for PW_{11}

The relative energies discussed above allow us to determine rather well the different adsorption modes on gold surfaces. However, it is more difficult to have a *quantitative* measure of the interaction between the POM and the surface. To analyze how strong the POM is attached to the gold surface, we have used two adsorption energies: E_{ads} and E'_{ads}. The former is the traditional adsorption energy, which is defined by eq. 1, where E_{tot} is the energy of the whole system, E_{surf} is the energy of the clean surface, and E_{KPOM} is the energy of the POM surrounded by

the counterions in its optimal distribution (model **A** in Table 1). On the other hand, E'_{ads} (eq. 2) differs from E_{ads} in the term E_{KPOM}. To determine E'_{ads}, the term E'_{KPOM} is computed considering the cation distribution of the POM when it is adsorbed. Hence, E'_{ads} can be understood as the minimum energy that is required to detach the POM from the gold surface.

$$E_{ads} = E_{tot} - E_{surf} - E_{KPOM} \quad \text{Eq. 1}$$

$$E'_{ads} = E_{tot} - E_{surf} - E'_{KPOM} \quad \text{Eq. 2}$$

Therefore, in vacuum, the surface represents a situation in which no water is present and the stabilization of the POM over-relies on both surface and cations. On the other hand, under the continuum solvent environment, the surface represents a fully hydrated situation that not only involves a potential over stabilization of the POM due to the inclusion of the implicit solvent, but also because it assumes that all the cations will be surrounding the adsorbate. In conclusion, these energies should not be taken as a quantitative reference but as a qualitative value.

Hence, E'_{ads} reflects a very exothermic adsorption in vacuum, between -17.0 and -30.0 kcal·mol^{-1}, although these values increase if we consider E_{ads} instead. This is because the cation's position has a strong influence in the energy of the whole system. Therefore, if we take as a reference a cation distribution that it is not the most stable, that will result in a lower adsorption energy, as shown in Table 3. In addition, the very exothermic values are an evidence of the over stabilizing role that the surface and the cations have on the "*dry*" surface.

Under "*wet*" conditions the situation is completely different. The E'_{ads} are now closer to 0 kcal·mol^{-1}, with the lowest energy being of only -5.1 kcal·mol^{-1} for the S_4-K. Indeed, this structure is the only one that shows exothermic E_{ads} (-2.5 kcal·mol^{-1}) whereas the rest of the adsorption modes owned very small but positive values. Thus, when the solvent is included, the polyoxometalate and the gold surface show a very weak interaction, which is consistent with the

experimental evidence that polyoxoanions like the $[SiW_{12}O_{40}]^{4-}$ spontaneously desorbs from the Au(111) surface after rinsing,[50] and are comparable to other oxo-systems adsorbed on gold as well, like the $AsMo_{11}VO_{40}^{4-}$, which has an estimated free energy of adsorption of –4.8 kcal·mol^{-1},[51] or the organomercaptan with an adsorption energy *ca*. -12 kcal·mol^{-1} from water onto gold.[52,53] We have also evaluated the *vdW* effects using DFT-D3 approach for the adsorption energies for S_4-K model in solution, however, the computed adsorption energies were found very large. Some more details are given in the supporting information (Table S1).

Table 3. Relative energies (ΔE) between different adsorbed systems and adsorption energies (E_{ads} *and* E_{ads}*'*) for the PW_{11} adsorbed on Au(100).

Adsorption Type	Vacuum			Solution		
	ΔE	E_{ads}	E'_{ads}	ΔE	E_{ads}	E'_{ads}
(1) S_4–K	1.2	0.5	-16.8	0.0	-2.5	-5.1
(2) S_4	11.3	10.4	-19.4	4.6	2.3	-4.6
(3) C_3–K	0.0	-0.7	-13.4	3.1	0.6	-2.2
(4) C_3	6.0	5.3	-18.0	6.7	4.2	-2.8
(5) Facing– K	3.2	2.5	-21.9	16.1	13.8	8.8
(6) Facing	30.2	29.3	-28.1	19.4	16.8	6.2

a) All values are in kcal·mol^{-1}.

Electronic structure

The electronic structure of the adsorbed POM in S_4-K is depicted in Figure 5 by means of the projected density of states (PDOS). In this representation, we have referred the energy range to

the energy of the Fermi level (E_F). Consequently, all bands found below 0 represent occupied orbitals whereas bands with positive energy mean virtual orbitals.

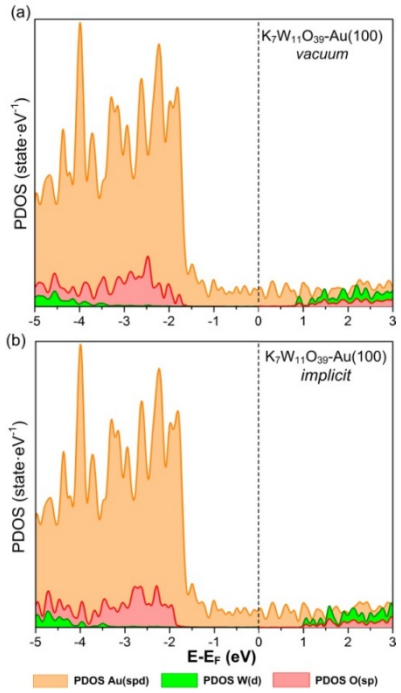

Figure 5. Projected density of states for system S_4-K in a) vacuum, and b) solvent. Similar results are obtained for C_3-K and Facing models in Figure S7.

The results obtained in vacuum and with implicit solvent are mainly the same. Electronic conduction undergoes through the gold surface in both cases, since this is the only contribution observed at the E_F (0 eV). Therefore, the POM does not play any role in the electronic conduction when it is adsorbed on gold. The only slightly difference between both situations is that the POM's conduction band, *i.e*. the front of the W(d) band, is found at 0.8 eV in the vacuum and at 1.0 eV in solution. This difference can be attributed to the stronger interaction between K and POM that exists in the vacuum that leads to an insignificant over-stabilization of these bands. Anyway, since the W(d) bands are not below the E_F, no charge transfer between surface and POM can occur. These results are in line with the calculated Bader charges listed in Table S1 of the ESI. The charge of the POM is –6.2 and –6.5 *e* for the vacuum and solvent respectively. This

charge is supplied by the counterions, as their total charge is 6.2 and 6.6 *e* respectively. This charge character was also evident by the calculated Mulliken populations shown in Table S2. Another common feature is the high polarization of the surface, as all layers are charged. Although this would indicate that more layers should be considered in our system, the surface polarization does not alter the main properties of the adsorbed POM. It should be noted that this polarization was also found for the free gold slab.

Finally, in order to consider the effects of explicit water on the electronic structure, we performed the optimization for S_t-K site by including the first solvation sphere, which was selected from a snapshot of a 2ns molecular dymamics simulation (Figure S6). In addition to the gold suface and the polyoxoanion, totally 46 water molecules and 7 K^+ are involved in the unit. The electronic structure of gold is almost not affected by the presence of explicit waters, and the position of W(d) and O(sp) bands show only 0.27 eV stabilization with respect to that in implicit solvent (Figure S8). Furthermore, the band gap between W(d) and O(sp) is well reproduced by introducing the implicit solvent (2.61 *versus* 2.65 eV in explicit water). It is worth mentioning that the calculations using explicit waters are much more computationally demanding, and that in this context to locate the overall energy minimum is very complicate because of the large number of local minima. Thus, the implicit solvent approach provides a much easier way to include the solvent effects in this type of studies.

Extending the modeling to $[SiW_{12}O_{40}]^{4-}$ on silver/gold surfaces

Finally, we have also analyzed the effect of the metal and the charge of the POM. To that end, we have performed calculations with the Ag(100) surface in both vacuum and solution, as well as studying the adsorption of the $[PW_{11}O_{39}]^{7-}$ and $[SiW_{12}O_{40}]^{4-}$. Notice that for the silver surface we

have used the gold surface unit cell, adjusting the cell parameter to a = 14.67Å, accordingly to our previously calculated bulk parameter for silver.[39,40] The adsorption mode for PW_{11} and SiW_{12} on Ag(100) is focused only on the S_4 orientation as discussed above.

Firstly, E'_{ads} shows the same trend we previously observed regarding to the magnitude of the adsorption energy when we consider the surface in vacuum and solution (Table 4). It is worth noting once again, that this difference arises from the over-stabilization role of the surface in the absence of the solvent. Interestingly, for all the systems, adsorption on silver is more favorable than on gold, although the magnitude of that stabilization depends on the POM.

For the PW_{11} and considering in vacuum, E'_{ads} is 5.6 kcal·mol^{-1} more stable for silver than for gold. With the solvent mediated, the adsorption energy is practically the same, -5.1 kcal·mol^{-1} for Au(100) and -5.8 kcal·mol^{-1} for Ag (100). The density of states for this system (Figure S9) suggests that there is no charge transfer between surface and POM regardless of the metal, which could explain why the adsorption energies are very similar for both metals.

The $[SiW_{12}O_{40}]^{4-}$ also has poor affinity with the Au(100) "*wet*" surface, with an adsorption energy of only -4.4 kcal·mol^{-1}, practically the similar energy obtained respect to the PW_{11} on gold. With silver surfaces, however, the affinity is much stronger, with an adsorption energy of -11.1 kcal·mol^{-1} (Table 4). The analysis of the DOS function shown in Figure S10 and the atomic charges which are listed in Table S1 clearly indicate that $[SiW_{12}O_{40}]^{4-}$ is spontaneously reduced when the anion is adsorbed on a solvated silver surface. This behavior is totally consistent with the experimental data reported by Gewirth[49] and also with our previous results, which combined classical MD simulations and DFT calculations.[25b] In other words, the continuum solvent model gives rise to the same results we obtained when we included explicit water molecules through MD simulations, but in an easiest way.

Table 4. Adsorption energy (E'_{ads}) computed for $[PW_{11}O_{39}]^{7-}$ and $[SiW_{12}O_{40}]^{4-}$ on Au(100) and Ag(100).[a)]

POMs	slab	Vac.	Sol.
PW_{11}	Au(100)	-16.8	-5.1
	Ag(100)	-22.4	-5.8
SiW_{12}	Au(100)	-12.2	-4.4
	Ag(100)	-21.2	-11.1

a) All values are in $kcal \cdot mol^{-1}$;

CONCLUSIONS

In this paper we have presented a general strategy based on periodic density functional theory and implicit solvent model to study the adsorption of highly charged species on surfaces. To that end, we investigated the adsorption orientation of the $[PW_{11}O_{39}]^{7-}$ anion on Au(100) by using a strategy that accounted for the charge of the system, the counterions and the solvent.

This approach involved compensating the charge of the POM by including explicit counterions in the calculations in order to ensure the electroneutrality of the system. The role of the implicit solvent was to stabilize all the ionic species involved in the solid-liquid interface, thus preventing an over-interaction between them. These considerations allowed the correct modelling of the adsorbate and ensured an accurate description of the adsorption itself.

In the particular case of study, the adsorption of $[PW_{11}O_{39}]^{7-}$ on Au (100), our calculations have revealed that unexpectedly, the POM does not adsorb through the lacuna, which is its more nucleophilic region, but it adsorbs on the surface in a similar fashion with respect to the atomic

connectivity as the non-defective $[SiW_{12}O_{40}]^{4-}$ anion on silver surfaces, supporting the critical role of cation-anion interactions in stabilizing the PW_{11}-monolayer.

Additionally, although the lacuna position is always filled with a counterion, the positions of the rest of the counterions around the POM do not influence the properties of the system. Notably, these findings are in agreement with the available experimental data.[8,19-21] We also computed the $[SiW_{12}O_{40}]^{4-}$ on Ag/Au(100) and the results were perfectly consistent with the experimental evidences and our previous calculations using a more expensive procedure.

Therefore, by using a highly charged system to test our model, we have demonstrated the efficiency and the robustness of our approach, which will be very helpful for the modelling of similar systems, as well as for the study of catalysis and electrocatalysis involving ionic species.

ASSOCIATED CONTENT

Supporting Information

The Supporting Information is available free of charge on the ACS Publications website at DOI:xxxxxxx

The Electronic Supporting Information contains: **1)** a discussion of the molecular dynamic simulation of $[PW_{11}O_{39}]^{7-}$ in solution; **2)** a description of the nomenclature for the counterions sites around the POM; **3)** supporting figure with the adsorbed models; **4)** Electrostatic Potential Map of free $[PW11O_{39}]^{7-}$; **5)** Representation of the supercell for S_4-K and Facing models; **6)** Molecular dynamic simulation for S_4-K adsorption; **7)** DOS analysis; and **8)** supporting tables for Bader charges and *vdw* correction discussion.

AUTHOR INFORMATION

Corresponding Author

*Email: anna.clotet@urv.cat; josepmaria.poblet@urv.cat

ACKNOWLEDGMENT

This work was supported by the Spanish Ministerio de Ciencia e Innovación (Project No. CTQ2014-52774-P) and the Generalitat de Catalunya (2014SGR-199 and XRQTC). JMP thanks the ICREA foundation for an ICREA ACADEMIA award. IAW thanks the ISF (190/13 and 152/11). The authors are grateful to COST Action CM1303 "Polyoxometalate Chemistry for Molecular Nanoscience (PoCheMoN)" for supporting this work, and XA-A also thanks the EPSRC for funding his research.

REFERENCES

(1) Pope, M. T. Heteropoly and Isopoly Oxometalates. Springer-Verlag: New York, 1983.

(2) Müller A.; Pope, M. T. Polyoxometalate Chemistry: From Topology via Self-Assembly to Applications, Kluwer, 2001.

(3) Long, D. L.; Burkholder, E.; Cronin, L. Polyoxometalate Clusters, Nanostructures and Materials: From Self Assembly to Designer Materials and Devices. *Chem. Soc. Rev.* **2007**, *36,* 105–121.

(4) Busche, C.; Vilà-Nadal, L.; Yan, J.; Miras, H. N.; Long, D. L.; Georgiev, V. P.; Asenov, A.; Pedersen, R. H.; Gadegaard; Mirza, N.M. M.; Paul, D.; Poblet, J. J. M.; Cronin, L. Design and fabrication of memory devices based on nanoscale polyoxometalate clusters. *Nature*. **2014**, *515,* 545–549.

(5) Lv, H.; Geletii, Y. V.; Zhao, C.; Vickers, J. W.; Zhu, G.; Luo, Z.; Song, J.; Lian, T.; Musaev, D. G.; Hill, C. L. Polyoxometalate Water Oxidation Catalysts and the Production of Green Fuel. *Chem. Soc. Rev.* **2012**, *41*, 7572–7589.

(6) Guo, S. X.; Liu, Y.; Lee, C.-Y.; Bond, A. M.; Zhang, J.; Geletii, Y. V.; Hill, C. L. Graphene-supported $[\{Ru_4O_4(OH)_2(H_2O)_4\}(\gamma\text{-}SiW_{10}O_{36})_2]^{10-}$ for Highly Efficient Electrocatalytic Water Oxidation. *Energy Environ. Sci.* **2013**, *6*, 2654–2663.

(7) Nishimoto, Y.; Yokogawa, D.; Yoshikawa, H.; Awaga, K.; Irle, S. Super-Reduced Polyoxometalates: Excellent Molecular Cluster Battery Components and Semipermeable Molecular Capacitors. *J. Am. Chem. Soc.* **2014**, *136*, 9042–9052.

(8) Wang, Y. F.; Weinstock, I. A. Polyoxometalate-decorated Nanoparticles. *Chem. Soc. Rev.* **2012**, *41*, 7479–7496.

(9) (a) Keita, B.; Nadjo, L. Activation of electrode surfaces: Application to the Electrocatalysis of the Hydrogen Evolution Reaction. *J. Electroanal. Chem.*, **1985**, *191*, 441– 448; (b) Keita, B.; Nadjo, L. Electrocatalysis by Electrodeposited Heteropolyanions and Isopolyanions. *J. Electroanal Chem.*, **1987**, *227*, 265–270; Keita; (c) B.; Nadjo, L.; Haeussler, J. P. Activation of Electrode Surfaces: Semiquantitative Characterization of Electrode Surfaces Modified with Heteropolyanions. *J. Electroanal. Chem.*, **1987**, *230*, 85–97; (d) Keita, B.; Nadjo, L. Surface Modifications with Heteropoly and Isopoly Oxometalates: Part III. Electrode Modification Procedures. the Necessity of Proton Interference During the Electrodeposition of the h.e.r. Catalysts. *J. Electroanal. Chem.*, **1988**, *247*, 157–172; (e) Keita, B.; Nadjo, L. Surface Modifications with Heteropoly and

Isopoly Oxometalates: Part I. Qualitative Aspects of the Activation of Electrode Surfaces Towards the Hydrogen Evolution Reaction. *J. Electroanal. Chem.,* **1988***, 243*, 87–103; (f) Keita, B.; Nadjo, L.; Saveant, J. M. Surface Modifications with Heteropoly and Isopoly Oxometalates: Part II. Electrocatalytic Behaviour of Glassy Carbon Surfaces Modified with 17-tungsto, 1-molybdo-diphosphate. *J. Electroanal. Chem.,* **1988***, 243*, 105–116.

(10) Rong, C.; Anson, F. C. Unusually Strong Adsorption of Highly Charged Heteropolytungstate Anions on Mercury Electrode Surface. *Anal. Chem.,* **1994***, 66,* 3124–3130.

(11) Ge, M.; Zhong, B.; Klemperer, W. G.; Gewirth, A. A. Self-Assembly of Silicotungstate Anions on Silver Surfaces. *J. Am. Chem. Soc.,* **1996***, 118*, 5812–5813.

(12) (a) Lee, L.; Wang, J. X.; Adzic, R. R.; Robinson, I. K.; Gewirth, A. A. Adsorption Configuration and Local Ordering of Silicotungstate Anions on Ag(100) Electrode Surfaces. *J. Am. Chem. Soc.,* **2001***, 123,* 8838–8843; (b) Lee, L.; Gewirth, A. A. Electrochemical Response of α-$H_4SiW_{12}O_{40}$ on Ag and Au Electrodes. *J. Electroanal. Chem.,* **2002***, 522,* 11–20; (c) Teague, C. M.; Li, X.; Biggin, M. E.; Lee, L.; Kim, J.;. Gewirth, A. A. Vibrational Spectroscopy of a Keggin Polyoxometalate on Metal Electrode Surfaces. *J. Phys. Chem. B,* **2004***, 108*, 1974–1985.

(13) (a) Lin, Y.; Finke, R. G. Novel Polyoxoanion- and Bu_4N^+-Stabilized, Isolable, and Redissolvable, 20-30-.ANG. Ir300-900 Nanoclusters: The Kinetically Controlled Synthesis, Characterization, and Mechanism of Formation of Organic Solvent-Soluble, Reproducible Size, and Reproducible Catalytic Activity Metal Nanoclusters. *J. Am. Chem.*

Soc., **1994**, *116 (18),* 8335–8353; (b) Lin, Y.; Finke, R. G. A More General Approach to Distinguishing "Homogeneous" from "Heterogeneous" Catalysis: Discovery of Polyoxoanion- and Bu_4N^+-Stabilized, Isolable and Redissolvable, High-Reactivity Ir.apprx.190-450 Nanocluster Catalysts. *Inorg*. *Chem*. **1994**,*33,* 4891–4910.

(14) Hsu-Yao T.; Browne, K. P.; Honesty, N; Tong, Y. J. Polyoxometalate-stabilized Pt Nanoparticles and Their Electrocatalytic Activities. *Phys*. *Chem*. *Chem*. *Phys*., **2011**, *13*, 7433–7438. (b) Li, S; Yu, X; Zhang, G; Ma, Y; Yao, J; Keita, B; Louis, N; Zhao, H. Green Chemical Decoration of Multiwalled Carbon Nanotubes with Polyoxometalate-Encapsulated Gold Nanoparticles: Visible Light Photocatalytic Activities *J*. *Mater*. *Chem*., **2011**, *21*, 2282–2287; (c) Corma, A; Iborra, S; Llabrés i Xamena, F. X; Montón, R; Calvino, J. J; Prestipino, C. Nanoparticles of Pd on Hybrid Polyoxometalate–Ionic Liquid Material: Synthesis, Characterization, and Catalytic Activity for Heck Reaction. *J*. *Phys*. *Chem*. *C,* **2010**, *114*, 8828–8836.

(15) Zhang, M. F.; Hao, J. C.; Neyman, A.; Wang, Y. F.; Weinstock, I. A. Influence of Polyoxometalate Protecting Ligands on Catalytic Aerobic Oxidation at the Surfaces of Gold Nanoparticles in Water, *Inorg*. *Chem*. DOI: 10.1021/acs.inorgchem.6b02167.

(16) Keita, B.; Liu, T. B.; Nadjo, L. Synthesis of remarkably stabilized metal nanostructures using polyoxometalates. *J*. *Mater*. *Chem*. **2009**, *19*, 19–33.

(17) Mitchell, S. G.; de la Fuente, J. M. The synergistic behavior of polyoxometalates and metal nanoparticles: from synthetic approaches to functional nanohybrid materials. *J*. *Mater*. *Chem*. **2012**, *22,* 18091–18100.

(18) Neyman, A.; Meshi, L.; Zeiri, L.; Weinstock, I. A. Direct Imaging of the Ligand Monolayer on an Anion-Protected Metal Nanoparticle through Cryogenic Trapping of its Solution-State Structure. *J. Am. Chem. Soc.,* **2008***, 130,* 16480–16481.

(19) Wang, Y. F.; Neyman, A.; Arkhangelsky, E.; Gitis, V.; Meshi, L.; Weinstock, I. A. Self-Assembly and Structure of Directly Imaged Inorganic-Anion Monolayers on a Gold Nanoparticle. *J. Am. Chem. Soc.,* **2009***, 131*, 17412–17422.

(20) Wang, Y. F.; Zeiri, O.; Sharet, S.; Weinstock, I. A. Role of the Alkali-Metal Cation Size in the Self-Assembly of Polyoxometalate-Monolayer Shells on Gold Nanoparticles. *Inorg. Chem.,* **2012***, 51*, 7436–7438.

(21) Sharet, S.; Sandars, E.; Wang, Y. F.; Zeiri, O.; Neyman, A.; Meshi, L.; Weinstock, I. A. Orientations of Polyoxometalate Anions on Gold Nanoparticles. *Dalton.Trans.,* **2012***, 41*, 9849-9851.

(22) Cameron, J. M.; Vila-Nadal, L.; Winter, R. S.; Iijima, F.; Murillo, J. C.; Rodríguez-Fortea, A.; Oshio, H.; Poblet, J. M.; Cronin, L. Investigating the Transformations of Polyoxoanions Using Mass Spectrometry and Molecular Dynamics. *J. Am. Chem. Soc.* **2016,** *138*, 8765–8773.

(23) Proust, A.; Matt, B.; Villanneau, R.; Guillemot, G.; Gouzerh, P.; Izzet, G. Functionalization and Post-functionalization: A Step Towards Polyoxometalate-based Materials. *Chem. Soc. Rev.* **2012**, *41*, 7605–7622.

(24) (a) Muñiz, J.; Cuentas-Gallegos, A. K.; Robles, M.; Valdéz, M. Bond Formation, Electronic Structure, and Energy Storage Properties on Polyoxometalate–carbon Nanocomposites. *Theor. Chem. Acc.* **2016**, *135*, 92; (b) Muñiz, J.; Celaya, C.; Mejía-Ozuna, A.; Cuentas-Gallegos, A. K.; Mejía-Mendoza, L. M.; Robles, M.; Valdéz, M. First Principles Study on the Electronic Structure Properties of Keggin Polyoxometalates on Carbon Substrates for Solid-state Devices. *Theor. Chem. Acc.* **2017**, *136*, 26.

(25) (a) Aparicio-Angles, X.; Clotet, A.; Bo, C.; Poblet, J. M. Towards the Computational Modelling of Polyoxoanions on Metal Surfaces: IR Spectrum Characterisation of $[SiW_{12}O_{40}]^{4-}$ on Ag(111). *Phys. Chem. Chem. Phys.*, **2011**, *13*, 15143–15147; (b) Aparicio-Angles, X.; Miro, P.; Clotet, A.; Bo, C.; Poblet, J. M. Polyoxometalates Adsorbed on Metallic Surfaces: Immediate Reduction of $[SiW_{12}O_{40}]^{4-}$ on Ag(100). *Chem. Sci.*, **2012,** 3, 2020–2027.

(26) Borzenko, M. I.; Nazmutdinov, R. R.; Glukhov, D. V.; Tsirlina, G. A.; Probst, M. Self-inhibition Phenomena in the Electroreduction of Hexamolybdocobaltate(III): A Combined Experimental and Computational study. *Chem. Phys.*, **2005**, *319*, 200–209.

(27) Rozanska, X.; Sautet, P.; Delbecq, F.; Lefebvre, F.; Borshch, S.; Chermette, H.; Basset, J.-M.; Grinenval, E. Polyoxometalate Grafting onto Silica: Stability Diagrams of $H_3PMo_{12}O_{40}$ on {001}, {101}, and {111} β-cristobalite Surfaces Analyzed by DFT. *Phys. Chem. Chem. Phys.*, **2011**, *13*, 15955–15959.

(28) (a) Wen, S. Z.; Guan, W.; Wang, J. P.; Lang, Z. L.; Yan, L. K.; Su, Z. M. Theoretical Investigation of Structural and Electronic Propertyies of $[PW_{12}O_{40}]^{3-}$ on Graphene Layer.

Dalton Trans., **2012**, *41*, 4602–4607; (b) Wen, S. Z.; Guan, W.; Kan, Y. H.; Yang, G. C.; Ma, N. N.; Yan, L.K.; Su, Z. M.; Chen, G. H. Theoretical Insights into $[PMo_{12}O_{40}]^{3-}$ Grafted on Single-walled Carbon Nanotubes. *Phys. Chem. Chem. Phys.*, **2013**, *15,* 9177–9185.

(29) Liu, R.; Zhang, G.; Cao, H.; Zhang, S.; Xie, Y.; Haider, A.; Kortz, U.; Chen, B.; Dalal, N. S.; Zhao, Y.; Zhi, L.; Wu, C.; Yan, L.; Su, Z.; Keita, B. Enhanced Proton and Electron Reservoir Abilities of Polyoxometalate Grafted on Graphene for High-performance Hydrogen Evolution. *Energy Environ. Sci.* **2016**, *9*, 1012–1023.

(30) (a) López, X.; Carbó, J. J.; Bo, C.; Poblet, J. M. Structure, Properties and Reactivity of Polyoxometalates: A Theoretical Pperspective. *Chem. Soc. Rev.* ***2012***, *41*, 7537-7571; (b) López, X.; Miró, P.; Carbó, J. J.; Rodríguez-Fortea, A.; Bo, C.; Poblet, J. M. Current Trends in the Computational Modelling of Polyoxometalates. *Theor. Chem Acc.* **2011**, *128*, 393–404.

(31) (a) Kresse, G.; Hafner, Ab initio Molecular Dynamics for Liquid Metals. J. *Phys. Rev. B: Condens. Matter,* **1993**, *47*, 558–561; Kresse, G.; Hafner, J. Ab initio Molecular-dynamics Simulation of the Liquid-metal–amorphous-semiconductor Transition in Germanium. *Phys. Rev. B: Condens. Matter,* **1994**, *49*, 14251–14269; (b) Kresse, G.; Furthmuller, J. Efficiency of ab-initio Total Energy Calculations for Metals and Semiconductors Using a Plane-wave Basis Set. *Comput. Mater. Sci.,* **1996**, *6*, 15–50; (c) Kresse, G.; Furthmuller, J. Efficient Iterative Schemes for Ab initio Total-energy Calculations Using a Plane-wave Basis Set. *Phys. Rev. B: Condens. Matter,* **1996**, *54*, 11169–11186.

(32) Perdew, J. P.; Chevary, J. A.; Vosko, S. H.; Jackson, K. A.; Pederson, M. R.; Singh, D. J.; Fiolhais, C. Atoms, molecules, solids, and surfaces: Applications of the Generalized Gradient Approximation for Exchange and Correlation. *Phys. Rev. B: Condens. Matter,* **1992**, *46*, 6671–6687.

(33) (a) Blöchl, P. E. Projector Augmented-wave Method. *Phys. Rev. B: Condens. Matter*, **1994**, *50*, 17953–17979; (b) Hafner, J. Ab-Initio Simulations of Materials Using VASP: Density-Functional Theory and Beyond. *J. Comput. Chem.,* **2008**, *29, 2044–2078*.

(34) Monkhorst, H. J.; Pack, J. D. Special Points for Brillouin-zone Integrations. *Phys. Rev. B: Solid State*, **1976**, *13*, 5188–5192.

(35) Bader, R. F. W. Atom in Molecules. A Quantum Theory, Oxford University Press, Oxford, 1990.

(36) Henkelman, G.; Arnaldsson, A.; Jonsson, H. A Fast and Robust Algorithm for Bader Decomposition of Charge Density. *Comput. Mater. Sci.,* **2006**, *36*, 354–360.

(37) Fishman, M.; Zhuang, H. L.; Mathew, K.; Dirschka, W.; Hennig, R. G. Accuracy of Exchange-correlation Functionals and Effect of Solvation on the Surface Energy of Copper. *Phys. Rev. B* **2013**, *87*, 245402-1–245402-7; Mathew, K.; Sundararaman, R.; Letchworth-Weaver, K.; Arias, T. A.; Hennig, R. G. Implicit Solvation Model for Density-functional Study of Nanocrystal Surfaces and Reaction Pathways. *J. Chem. Phys.* **2014**, *140*, 084106-1–084106-8.

(38) Álvarez-Moreno, M.; de Graaf, C.; López, N.; Maseras, F.; Poblet, J.M.; Bo, C. Managing the Computational Chemistry Big Data Problem: The ioChem-BD Platform. *J. Chem. Inf. Model.* **2015**, *55*, 95–103.

(39) Elliot, S. *Physics of Amorphous Materials*, 2nd revised edition ed., 1990.

(40) Hook, J. R.; Hall, H. E. *Solid State Pysics*, 2nd Edition ed., Wiley, 1995.

(41) Smith, W.; Forester, T. R. DL_POLY_2.0: A General-purpose Parallel Molecular Dynamics Simulation Package. *J. Mol. Graphics Modell.*, **1996**, *14*, 136–141.

(42) Martınez, L.; Andrade, R.; Birgin, E. G.; Martınez, J. M. PACKMOL: A Package for Building Initial Configurations for Molecular Dynamics Simulations. *J. Comput. Chem.*, **2009**, *30*, 2157–2164.

(43) Jorgensen, W. Comparison of Simple Potential Functions for Simulating Liquid Water. J. *Chem. Phys.*, **1983**, *79*, 926–935.

(44) Leroy, F.; Miro, P.; Poblet, J. M.; Bo, C.; Avalos, J. B. Keggin Polyoxoanions in Aqueous Solution: Ion Pairing and Its Effect on Dynamic Properties by Molecular Dynamics Simulations. *J. Phys. Chem. B,* **2008**, *112*, 8591–8599.

(45) Miró, P.; Poblet, J. M.; Ávalos, J. B.; Bo, C. Towards a Computational Treatment of Polyoxometalates in Solution Using QM Methods and Explicit Solvent Molecules. *Can. J. Chem.*, **2009**, 1296–1301.

(46) Schreiber, R. E.; Houben, L.; Wolf, S. G.; Leitus, G.; Lang, Z.-L.; Carbó, J. J.; Poblet, J. M.; Neumann, R. Real-time molecular scale observation of crystal formation. *Nature Chem*. doi:10.1038/nchem.2675.

(47) Solé-Daura, A; Goovaerts, V.; Stroobants, K.; Absillis, G.; Jiménez-Lozano, P.; Poblet, J. M.; Hirst, J. D.; Parac-Vogt, T. N.; Carbó, J. J. Probing Polyoxometalate–Protein Interactions Using Molecular Dynamics Simulations, *Chem. Eur. J.* **2016**, 22, 15280-15289.

(48) Graham, C. R.; Ott, L. S.; Finke, R. G. Ranking the Lacunary $(Bu_4N)_9\{H[\alpha_2\text{-}P_2W_{17}O_{61}]\}$ Polyoxometalate's Stabilizing Ability for Ir(0)n Nanocluster Formation and Stabilization Using the Five-Criteria Method Plus Necessary Control Experiments. *Langmuir* **2009**, *25*, 1327–1336.

(49) Momma, K.; Izumi, F. *VESTA*: A Three-dimensional Visualization System for Electronic and Structural Analysis. *J. Appl. Cryst.* **2008**, **41**, 653-658.

(50) Lee, L.; Gewirth, A. A. Electrochemical Response of $\alpha\text{-}H_4SiW_{12}O_{40}$ on Ag and Au Electrodes. *J. Electroanal. Chem*. **2002**, *522*, 11–20.

(51) Tang, Z. Y.; Liu, S.Q.; Wang, E.K.; Dong, S. J. Self-Assembled Monolayer of Polyoxometalate on Gold Surfaces: Quartz Crystal Microbalance, Electrochemistry, and in-Situ Scanning Tunneling Microscopy Study. *Langmuir*, **2000**, *16*, 4946–4952.

(52) Kirk, J. S.; Bohn, P. W. Surface Adsorption and Transfer of Organomercaptans to Colloidal Gold and Direct Identification by Matrix Assisted Laser Desorption/Ionization Mass Spectrometry. *J. Am. Chem. Soc.,* **2004**, *126*, 5920–5926.

(53) Schessler, H. M.; Karpovich, D. S.; Blanchard, G. J. Quantitating the Balance between Enthalpic and Entropic Forces in Alkanethiol/Gold Monolayer Self Assembly. *J. Am. Chem. Soc.*, **1996**, *118*, 9645–9651.

Table of Content

Counter-intuitive Adsorption of $[PW_{11}O_{39}]^{7-}$ on Au(100)

Zhongling Lang,[1] Xavier Aparicio-Anglès,[2] Ira Weinstock,[3] Anna Clotet, [1]* and Josep M. Poblet[1]*

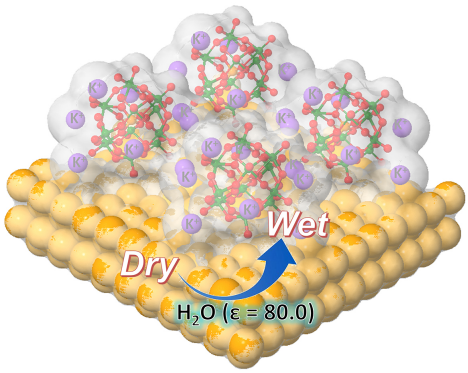

Highly charged polyoxometalates adsorbed on gold surface were modeled by using periodic DFT to provide a general modelling strategy for POMs-metallic surface materials.